HARDWARE-ACCELERATED WEB VISUALIZATION OF VECTOR FIELDS. CASE STUDY IN OCEANIC CURRENTS

Mauricio Aristizabal[1], John Congote[1,2], Alvaro Segura[2], Aitor Moreno[2], Harbil Arregui[2] and Oscar Ruiz[1]

[1]*CAD/CAM/CAE Laboratory, EAFIT University, Medellin, Colombia*

[2]*Vicomtech Research Center, Donostia - San Sebastian, Spain*

maristi7@eafit.edu.co, {jcongote,asegura,amoreno,harregui}@vicomtech.org, oruiz@eafit.edu.co

Keywords: Line Integral Convolution, Hierarchical Integration, Flow Visualization, WebGL

Abstract: Visualization of vector fields plays an important role in research activities nowadays. Increasing web applications allow a fast, multi-platform and multi-device access to data. As a result, web applications must be optimized in order to be performed heterogeneously as well as on high-performance as on low capacity devices. This paper presents a hardware-accelerated scheme for integration-based flow visualization techniques, based on a hierarchical integration procedure which reduces the computational effort of the algorithm from linear to logarithmic, compared to serial integration methodologies. The contribution relies on the fact that the optimization is only implemented using the graphics application programming interface (API), instead of requiring additional APIs or plug-ins. This is achieved by using images as data storing elements instead of graphical information matrices. A case study in oceanic currents is implemented, showing that the procedure requires 32 integration steps to obtain good visual results.

GLOSSARY

API	Application Programming Interface
CUDA	Compute Unified Device Architecture
PL	Piecewise Linear
SIMD	Single Instruction Multiple Data
GLSL	Graphic Library Shading Language
WebGL	Web Graphic Library
LIC	Line Integral Convolution
GPU	Graphics Processing Unit
FBO	FrameBufer Object
Shader	Instructions to be performed in the GPU

1 INTRODUCTION

Vector field visualization has an important role in the automotive and aero-spatial industries, maritime transport, engineering activities and others. It allows the detection of particularities of the field such as vortexes or eddies in flow fields, but also permits exploring the entire field behavior, determining stream paths.

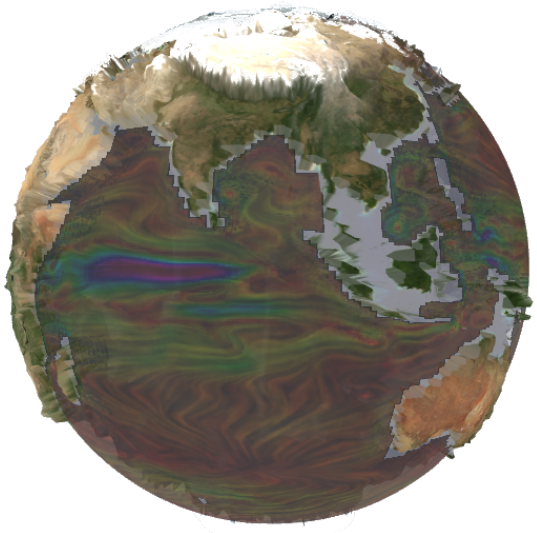

Figure 1: LIC flow visualization of Indian ocean currents in WebGL. Hierarchical integration was used to reduce the total number of iterations required to calculate the integrals, reducing it from 32 to four iterations.

Particularly, ocean flow visualization is an important factor in weather and climate prediction activities since the movement of huge water masses can pro-

duce temperature variation of wind currents.

As a result, flow visualization of oceanic streams becomes an important activity to represent the ocean's behavior. There exist several methodologies for this purpose, like geometric-based methodologies, which use objects whose visual properties (like size and color) represents the flow characteristics. However their placement along the field is determinant to visualize anomalies as eddies or vortexes, and, therefore, data preprocessing is required. On the other hand, there are texture-based approaches, which modifies or creates textures to represent the flow's behavior.

LIC convolves a noise field with a mapping image along the trajectory of each particle in the vector field. It is a widely implemented texture-based procedure, and can easily detect flow's anomalies without data preprocessing since a quasi-continuous visualization is performed. However, as for the procedure to be accurate, several evaluations of textures are required in order to numerically build an integral, and therefore it increases the computation time of the procedure.

The emerging technology WebGL (OpenGL for the web), allows hardware-accelerated visual applications to be performed in web-pages. However, challenges arise since these applications must be suitable to be executed in low capacity devices such as mobile devices, smart phones and tablet computers. As a consequence, LIC flow visualization might not be suitable for this technology unless optimization procedures are applied.

Our contribution is a hardware-accelerated optimization scheme for LIC flow visualization implemented in WebGL. The optimization is based on a hierarchical integration procedure (Hlawatsch et al., 2011), which reuses previously calculated information in order to build the integrals and therefore avoids unnecessary calculations. As a consequence the complexity of the procedure is reduced, compared with a serial calculation of integrals, from $O(N)$ to $O(\log N)$ (Hlawatsch et al., 2011) Compared with other methodologies, our implementation only requires WebGL API to be performed, as it employs images as data storing elements instead of graphical information matrices, using the render-to-texture capabilities of WebGL. The optimization is purely implemented on shaders, this is, in GPU's hardware, which allows to the procedure to have a fast and parallel processing scheme.

This paper is organized as follows. Section 2 presents the related work. Section 3 exposes the methodology of LIC flow visualization and its optimization. Section 4 presents a case of study in oceanic currents and finally the conclusions of our work are presented in section 5.

2 LITERATURE REVIEW

2.1 Flow Visualization

A great amount of methodologies to visualize vector fields (flow fields) has been developed among the last decades. Geometric-based approaches draw icons on the screen whose characteristics represent the behavior of the flow (as velocity magnitude, vorticity, etc). Examples of these methodologies are arrow grids (Klassen and Harrington, 1991), streamlines (Kenwright and Mallinson, 1992) and streaklines (Lane, 1994). However, as these are discrete approaches, the placement of each object is critical to detect the flow's anomalies (such as vortexes or eddies), and therefore, data preprocessing is needed to perform an illustrative flow visualization. Reference (McLoughlin et al., 2010) presents an up-to-date survey on geometric-based approaches.

On the other hand, texture-based approaches represent both a more dense and a more accurate visualization, which can easily deal with the flow's feature representation as a dense and semi-continuous (in stead of sparse and discrete) flow visualization is produced. A deep survey in the topic on texture-based flow visualization techniques is presented by (Laramee et al., 2004).

Reference (Van Wijk, 2002) implements an animated flow visualization technique in which a noise image is bended out by the vector field, and then blended with a number of background images. In (Van Wijk, 2003) the images are then mapped to a curved surface, in which the transformed image visualizes the superficial flow.

Line Integral Convolution (LIC), presented by (Cabral and Leedom, 1993), is a widely implemented texture-based flow visualization procedure. It convolves the associated texture-pixels (texels) with some noise field (usually a white noise image) over the trajectory of each texel in some vector field. This methodology has been extended to represent animated (Forssell and Cohen, 1995), 3D (Liu and Moorhead II, 2004) and time varying (Liu and Moorhead, 2005; Liu and Moorhead II, 2004) flow fields.

An acceleration scheme for integration-based flow visualization techniques is presented by (Hlawatsch et al., 2011). The optimization relies on the fact that the integral curves (such as LIC) are hierarchically constructed using previously calculated data, and, therefore, avoid unnecessary calculations. As a result, the computational effort is reduced, compared to serial integration techniques, from linear to logarithmic. Its implementation is performed on the

CUDA architecture, which allows a GPU-based parallel computing scheme, and therefore the computation time is critically reduced. However, it requires, additionally to the graphic APIs, the CUDA API in order to reuse data, and hence, execute the procedure.

2.2 WebGL literature review

The Khronos Group released the WebGL 1.0 Specification in 2011. It is a JavaScript binding of OpenGL ES 2.0 API and allows a direct access to GPU graphical parallel computation from a web-page. Calls to the API are relatively simple and its implementation does not require the installation of external plug-ins, allowing an easy deployment of multi-platform and multi-device applications. However, no data calculated on shaders but images can be transfered between rendering procedures using FBOs.

Several WebGL implementations of different applications have been done such as volume rendering, presented by (Congote et al., 2011) or visualization of biological data, presented by (Callieri et al., 2010). However, for the best of our knowledge, no other implementation that regards to LIC flow visualization on WebGL has been found in the literature or in the Web.

2.3 Conclusion of the Literature Review

WebGL implementations allow to perform applications for heterogeneous architectures in a wide range of devices from low-capacity smart phones to high-performance workstations, without any external requirement of plug-ins or applets. As a result, optimized applications must be developed. In response to that, this work optimizes the visualization of 2D steady vector fields using images as data storing elements instead of graphical information matrices. As a consequence, previously calculated data is reused, avoiding unnecessary calculations, and reducing the complexity of the algorithm to $O(\log N)$. Hence, only the graphics API is required for its implementation, preserving the multi-platform purpose of the application.

3 METHODOLOGY

This article addresses the optimization of integration-based flow visualization procedures using only the graphics API. It starts from a 2D vector field $F : X \to \mathbb{R}^2$, with $X \subseteq \mathbb{R}^2$, representing the velocity at each point inside the field. An image represented as the 2D matrix $M : [1,h_M] \times [1,w_M] \to (R,G,B,A)$, with h_M and w_M representing its height and width respectively in pixels, and a noise field $W : \mathbb{R}^2 \to \mathbb{R}$, both mapping to F.

The goal is to calculate a 2D matrix $\bar{I} : [1,h_I] \times [1,w_I] \to (R,G,B,A)$ that defines an image, with h_I and w_I representing its height and width in pixels. Each pixel is a four-component vector (R,G,B,A) of red, green, blue and alpha values $(R,G,B,A \in [0,1])$.

3.1 Line Integral Convolution

In order to visualize 2D vector field, the procedure convolves the mapping image M with its noise field W along the trajectory of each point in the vector field, as proposed by (Cabral and Leedom, 1993). For this purpose, let us define q as an arbitrary point in the field. Hence, for its associated finite trajectory c (extracted from F), with $p(s) \in c$, and s the parameter associated to c, the resulting image is obtained as follows:

$$\overline{I(q)} = \frac{\int_c M(p(s))W(p(s))ds}{\int_c W(p(s))ds} \tag{1}$$

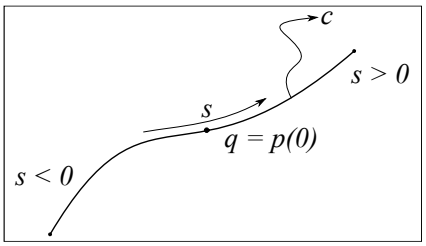

Figure 2: Trajectory of the point p inside F.

Note that q represents the starting point of the trajectory that is going to be convolved (i.e. $p(0) = q$), and the trajectory c evaluates the upstream ($s > 0$) and downstream ($s < 0$) directions. This integral is performed for all $q \in X$

For a computer implementation, a discrete calculation of the integral is required. As a result, a PL approximation of c is performed using a first-order approximation of the point's displacement (see equations 2-5). Figure 3 shows the PL approximation of c.

$$p_j(1) = p_j(0) + k\frac{F(p_j(0))}{\|F(p_j(0))\|} \tag{2}$$

$$p_j(2) = p_j(1) + k\frac{F(p_j(1))}{\|F(p_j(1))\|} \tag{3}$$

$$p_j(-1) = p_j(0) - k\frac{F(p_j(0))}{\|F(p_j(0))\|} \tag{4}$$

$$p_j(-2) = p_j(-1) - k\frac{F(p_j(-1))}{\|F(p_j(-1))\|} \tag{5}$$

In equations (2-5), only the direction of the velocity is regarded. The parameter k represents a scaling

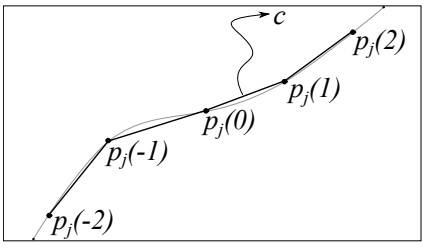

Figure 3: Piecewise linear approximation of c.

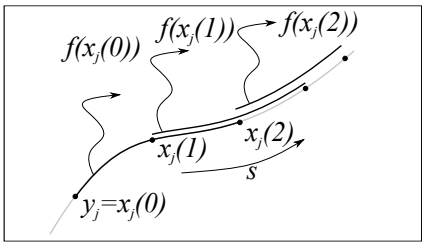

Figure 4: Trajectory overlapping in line integral evaluation.

factor of the displacement, in order to transform that vector to the local coordinates of the representation. With this, the final image $\bar{I}$ is calculated for each point q_j in the field as follows.

$$I_U(q_j) = \sum_{i=1}^{t} M(p_j(i))W(p_j(i)) \tag{6}$$

$$I_D(q_j) = \sum_{i=1}^{t} M(p_j(-i))W(p_j(-i)) \tag{7}$$

$$P_U(q_j) = \sum_{i=1}^{t} W(p_j(i)) \tag{8}$$

$$P_D(q_j) = \sum_{i=1}^{t} W(p_j(-i)) \tag{9}$$

$$\overline{I(q_j)} = \frac{I_U(q_j) + I_D(q_j)}{P_U(q_j) + P_D(q_j)} \tag{10}$$

where I_U and I_D represents the convolution between M and W in the upstream and downstream directions respectively, P_U and P_D represents the total weight sum in both directions in order to average the convolution, t represents the maximum number of integration steps for both directions and q_j represents the current evaluating point.

3.2 Hierarchical Integration

Integration over massive point trajectories in n-dimensional vector fields suffer from unnecessary step calculations since several points in the field might lie over the same trajectory and therefore share portions of the integrals. Figure 4 illustrates this situation for different points along the same path. In response to this, hierarchical integration (Hlawatsch et al., 2011) only calculates the necessary steps and then iteratively grows the integrals reusing the data, reducing the computational complexity of the algorithm from $O(N)$, using serial integration methodology, to $O(\log N)$. The procedure is summarized as follows.

Let us define some arbitrary line integral $f : Y \to \mathbb{R}^m$, with $Y \subseteq \mathbb{R}^n$, bounded by its trajectory c, and its discrete approximation like described in equation 11.

$$f(y_j) = \int_c w(x_j(s))ds \approx \sum_{i=1}^{t} w(x_j(i))\Delta s \tag{11}$$

where t is is the maximum number of steps, representing the curve length, $x_j(0) = y_j$ is the starting point of the trajectory path. The integration procedure is performed for all points $y_j \in Y$ in parallel.

For the sake of simplicity assume that $\Delta s = 1$, $\forall y_j \in Y$ and therefore $f(y_j) \approx \sum_{i=1}^{t} w(x_j(i))$. The algorithm starts with the calculation of the first integration step for all the points in the field, this is:

$$f_0(y_j) = w(x_j(1)) \tag{12}$$

It is required to store the last evaluated point $x_j(1)$ over the growing trajectory and the value of $f_1(y_j)$ for every point in order to reuse them in the following steps to build the integral. With this, the following is to update the value of the integral, using the sum of the previously calculated step at y_j and the step evaluated at its end point ($x_j(1)$), namely,

$$f_1(y_j) = f_0(x_j(0)) + f_0(x_j(1)) \tag{13}$$

In this case, the end point of $f_1(x_j(0))$ is $x_j(2)$ as the calculation evaluates $f_0(x_j(1))$, and therefore the next iteration must evaluate f at $x_j(0)$ and $x_j(2)$ in order to grow the integral. In general, the k'th iteration of the procedure is calculated as

$$f_k(y_j) = f_{k-1}(x_j(0)) + f_{k-1}(x_j(end)) \tag{14}$$

Note that each iteration of this procedure evaluates two times the integration steps evaluated in the previous iteration. As a result, the total number of integration steps t must be a power of two, and the hierarchical iterations required to achieve this evaluations is reduced by a logarithmic scale. This is, the total number of iterations to be performed $k = \log_2 t$. Figure 5 illustrates the procedure for two hierarchical iterations, which leads to four integration steps to build the integral.

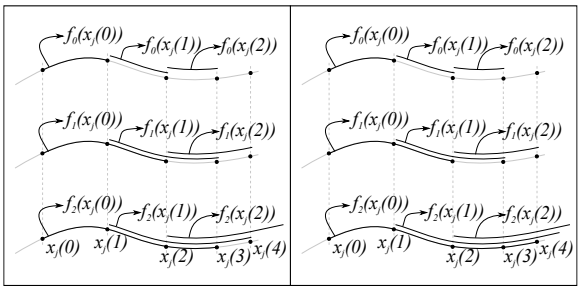

Figure 5: Comparison between the growth of the evaluated trajectories using serial integration methodology (left) and the hierarchical integration procedure (right), for iterations k equals to 0, 1 and 2.

3.3 Data Storing

Despite graphics APIs does not allow to transfer data calculated on shaders (such as matrices, vectors or single values), between rendering procedures, they can transfer images. An image is a 2D matrix that stores at each position a four-component vector that defines its color, i.e. $[1,h]\times[1,w]\rightarrow(R,G,B,A)$, with h and w its height and width in pixels respectively. A pixel color is defined by red, green blue and alpha values ($R,G,B,A\in[0,1]$).

As a result, for any field $X\in\mathbb{R}^2$ it is possible to store four values associated to any point $p_j\in X$ in an image that maps to X. Note that pixels are discrete values and p_j might be continuous. In this case, average and interpolation of data are required to both read and write the values on the image that maps to the field, and therefore avoid high error between calculations. If more than four values are required to be stored, it is needed to render (calculate) more than one image in order to store those values.

4 CASE STUDY

In this section the visualization of oceanic currents in a WebGL application using a hierarchical integration scheme is carried out. Images are used to transfer data between iterations and to input the ocean's velocity field, the ocean's bathymetric and the earth's topographic information.

4.1 Global Information

Many data services regards to the measurement of earth's information such as wind flow, superficial temperature, ocean salinity and others. For this application, the vector field that defines the velocity is required. The Global Ocean Data Assimilation System (GODAS)[1] provides this information in a netCDF format (Hankin et al., 2010), which allows, throughout servers, to visualize the data as an image information. Figures 6(a) and 6(b) shows the ocean's longitudinal and latitudinal components of the velocities respectively, in grayscale images. They represent for a full white color (R=G=B=1.0) a velocity component of 3.0 and for a full black color (R=G=B=0.0) a velocity component of -3.0.

Earth's bathymetric (B) and topographic (T) information, provided by the NASA's earth observatory[2], refers to the ocean's depth and the land's height respectively, and is also stored as images (see Figures 6(c) and 6(d)). For bathymetric information, brighter values represent shallow water. In contrast, for topographic information, brighter values represent higher surface elevation. As a result, these data are used to transform earth's vertices, which initially represent a sphere. For vertex $V(q_j)$, its transformation is carried out as follows,

$$V(q_j)=V(q_j)*(1-\alpha_B\,B(q_j).R),\ \forall q_j\in X_{ocean} \quad (15)$$

$$V(q_j)=V(q_j)*(1+\alpha_T\,T(q_j).R),\ \forall q_j\in X_{land} \quad (16)$$

where α_B and α_T are user defined scaling factors to interactively vary the representation and X_{ocean} and X_{land} are the corresponding ocean and land regions respectively such that $X_{ocean}\cup X_{land}=X$ and $X_{ocean}\cap X_{land}=\emptyset$

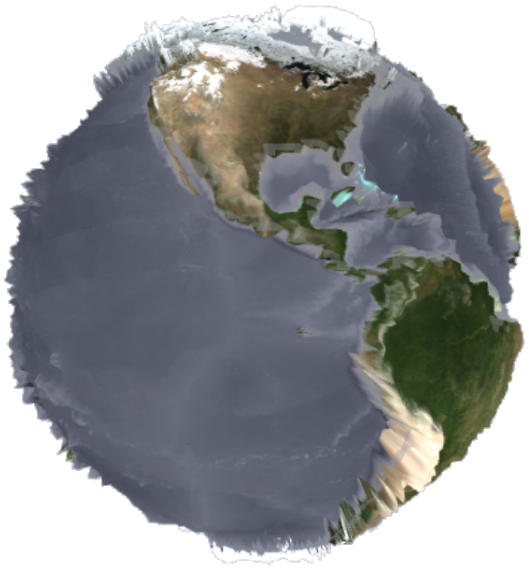

Figure 7: Earth vertex transformation using bathymetric and topographic information.

Finally, a satellite image of earth's surface (see figure 6(e)), also provided by the NASA's earth ob-

[1] *http://www.esrl.noaa.gov/psd/*

[2] *http://earthobservatory.nasa.gov/*

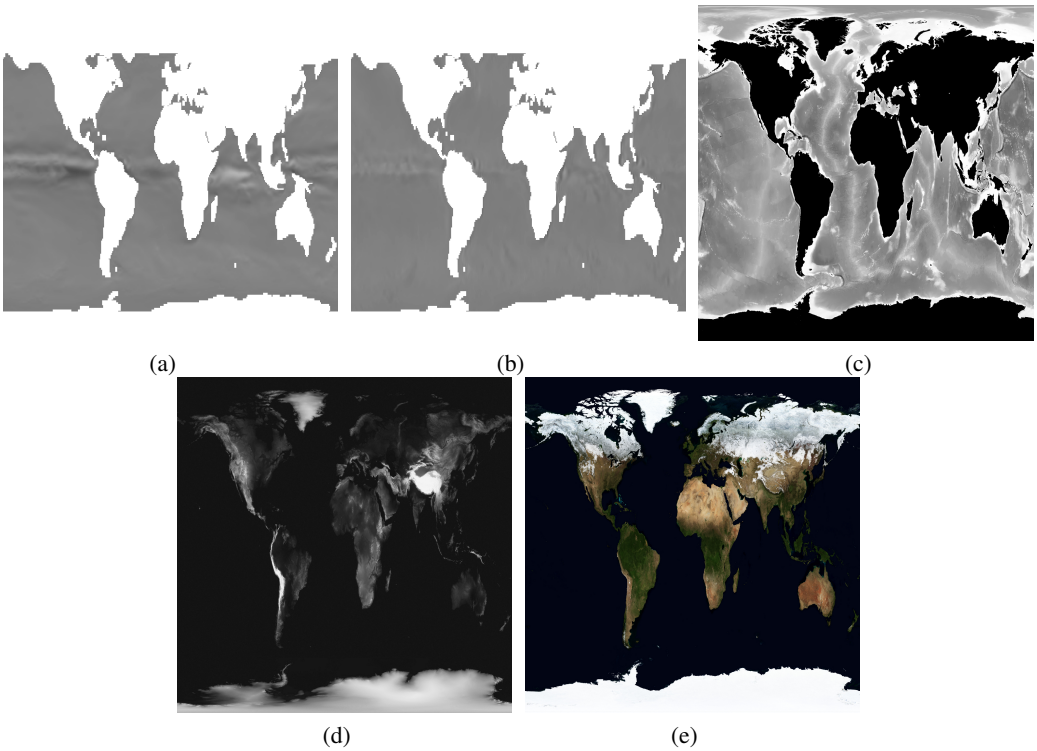

Figure 6: Global information. Gray-scale of the oceanic currents magnitude in the (a) longitudinal and (b) latitudinal directions, of the 1^{st} December of 2010. Gray-scale of the (c) bathymetric and (d) topographic information, and (e) satellite photography of earth.

servatory, is used to map the non-oceanic regions of the visualization.

4.2 Data Storing

Taking advantage of massive parallel computing capabilities and data interpolation of SIMD programming architectures, it is possible to optimize the calculation of the integrals using images. Although graphic libraries can not return or store previously calculated data as arbitrary matrices, they are capable of performing render-to-texture operations. This allows to store a rendered image in GPU's memory instead of displaying it, to then access it from another rendering procedure and access its information. As a result, images might be used as data storing elements instead of graphical information matrices.

In order to implement hierarchical integration with LIC, regarding that it performs a single direction integration and the integrals must be performed along both upstream and downstream directions, it is required to perform integration for both directions separately and then merge both results in order to obtain the final image $\bar{I}$.

The mapping image (M) used in this case study is shown in figure 8. It is a gray-scale image, therefore the values of each color components are the same for each pixel, i.e. $R = G = B$. The weight field used is $W(q_j) = 1.0 \ \forall q_j \in X$. In order to perform LIC with hierarchical integration, for both the upstream and downstream directions, one value is needed to store the partial integral (since M is single-valued), and two values are required to store the two coordinates that define the final point of the partially evaluated trajectory. As a consequence, two images are required to store the values for each point p_j in the field. For this purpose let us define the following convention of data storing in the next two images in order to store the data:

Image $Q : [1, h_Q] \times [1, w_Q] \rightarrow (R, G, B, A)$, is used to store the data in the upstream direction for each point q_j in the field. The first component (where the red component is stored) is used to store the partially evaluated convolution and the second and third components (green and blue components) store the coordinates of the tail point of the trajectory. The fourth component is always used as 1.0. Note that since the weight field is 1.0 for all points in the field, the convolution becomes the average of all values of M along the partially evaluated trajectory. As a result, the update throughout the iterations of the image is calcu-

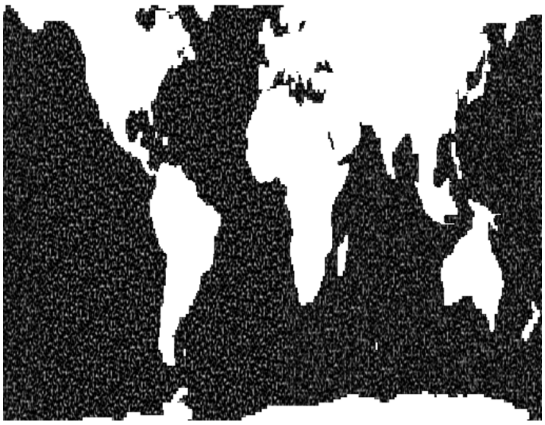

Figure 8: Mapping image to perform LIC.

lated as follows

$$Q_k(q_j) = \begin{bmatrix} \frac{Q_{k-1}(p_j(0)).R + Q_{k-1}(p_j(end)).R}{2} \\ Q_{k-1}(p_j(end)).G \\ Q_{k-1}(p_j(end)).B \end{bmatrix} \quad (17)$$

where $.R$, $.G$ and $.B$ extracts the values stored in the red, green and blue components of the image respectively.

With the same convention of Q, image $S : [1, h_Q] \times [1, w_Q] \rightarrow (R,G,B,A)$, is used to store the data but for the downstream direction for each point q_j in the field,

$$S_k(q_j) = \begin{bmatrix} \frac{S_{k-1}(p_j(0)).R + S_{k-1}(p_j(-end)).R}{2} \\ S_{k-1}(p_j(-end)).G \\ S_{k-1}(p_j(-end)).B \end{bmatrix} \quad (18)$$

As a consequence, the final visualization of the flow is calculated as follows

$$\overline{I(q_j)} = \frac{Q(q_j).R + S(q_j).R}{2} \quad (19)$$

4.3 Data Storage in WebGL

WebGL permits to set up vertex and index buffers, to change rendering engine state such as active texture units or transform matrices, and to invoke drawing primitives. It also allows to perform render-to-texture operations using FrameBuffer Objects (FBOs), which allow other render engines to access previously calculated data, all inside the GPU. Recently, while the research of this article was ongoing, the Khronos group released the OES_texture_float extension revision 3, which allows floating points texture management as color attachments in FBOs. This enables to store and reuse data inside the GPU's hardware, with floating point precision values, instead of 8-bit integers.

In order to perform render-to-texture operations in WebGL it is needed to define the necessary FBOs. Each FBO has an associated texture (image) to which the rendering code is performed. Additionally, for the matter of this implementation, it is important to consider that when the rendering procedure of an FBO is being performed, it does not allow to access the same memory space (in GPU) to which the rendering operation will write the information.

As a result, the flow visualization, regarding the hierarchical integration, requires the double of FBOs than the number of rendered images, this is, one FBO is used to calculate and update the image and the other FBO is used to copy the resulting image in another place of memory in order to allow data to be reused for the next iteration. Hence 4 FBOs are required to perform LIC flow visualization for this case study.

4.4 Flow Visualization in WebGL

Final results are shown in figure 9. The final LIC image $\bar{I}$ is used to determine the brightness of each point in the field. Color-mapping is determined by the speed at each point in a warm-cold color-scale.

Final results show that 5 iterations (see figure 9(f)) produce excessive blending that results in a blurred visualization and hence makes harder to detect streams (figure 10(c)). On the other hand, 3 iterations (see figure 9(d)) produce short paths, and therefore the identification of the flow's behavior is difficult (figure 10(a)). Optimal results are obtained after 4 hierarchical iterations (see figure 9(e)), this is, 16 total integration steps for both the upstream and downstream directions, making a detailed visualization with long and distinguishable trajectories (figure 10(b)).

5 CONCLUSIONS AND FUTURE WORK

This article presents a hardware accelerated LIC flow visualization in WebGL. The procedure is suitable to be performed on multi-platform and in low-capacity devices such as smart phones and tablet computers since no other API or plug-in is required to perform the procedure, and the number of iterations that is usually required is reduced. The procedure is not only suitable for WebGL implementation but for any render-to-texture capable parallel graphics implementation.

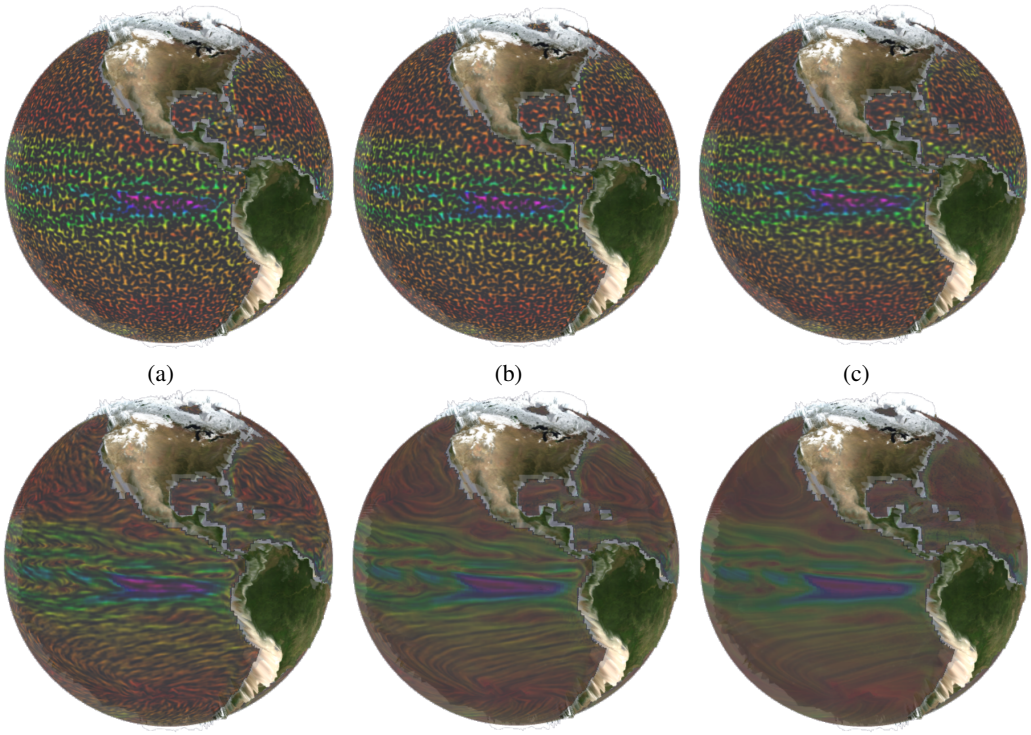

(a) (b) (c)

(d) (e) (f)

Figure 9: Visualization of the Pacific and Atlantic oceans currents using LIC with hierarchical line integration in WebGL. The initial iteration (a) shows only two integration steps, taking into account both integration directions (upstream and downstream). One iteration (b) achieves four integration steps. Two iterations (c) perform eight integration steps, which shows extremely short paths and streams are not detected. Three iterations (d) perform 16 integration steps and streams are barely detected. Four iterations (e) achieve 32 integration steps and shows distinguishable streams. Five iterations (f) performs 64 integration steps and show excessive blending.

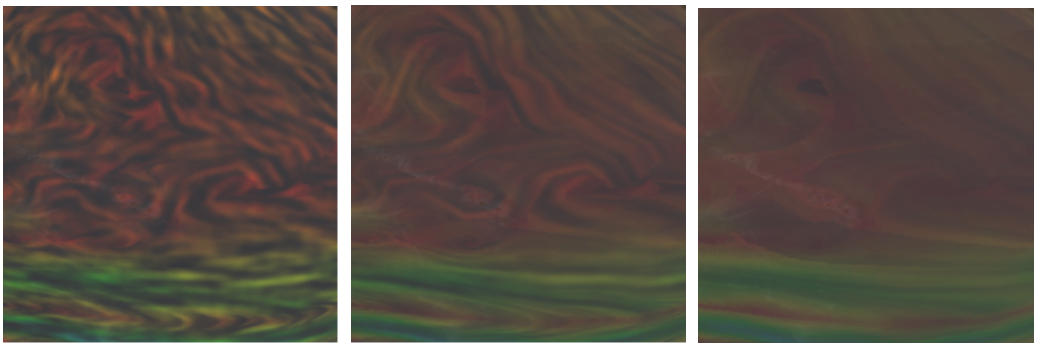

(a) (b) (c)

Figure 10: Comparison between different hierarchical iteration results. With 3 iterations (a) the visualization shows short paths and visual detection of streams is difficult, 4 iterations (b) show long and distinguishable paths and 5 iterations(c) shows excessive blending and detection of streams is difficult.

Results show that 32 effective integration steps (16 in both the upstream and the downstream directions) are required in order to obtain a desirable visualization. Our methodology decreases to only 4 real iterations the execution of the procedure, hence, significantly reducing the computational effort of the procedure.

It is proposed the development of a human user interaction application for the visualization of oceanic currents as a subsequent activity to this work. Apart from this, other topics might be suitable as future work such as the implementation of this methodology to visualize 3D vector fields and to other integration-based visual applications.

ACKNOWLEDGEMENTS

This work was partially supported by the Basque Government's ETORTEK Project (ITSASEUSII) research program and CAD/CAM/CAE Laboratory at EAFIT University and the Colombian Council for Science and Technology COLCIENCIAS. GODAS data (ocean velocity information) was provided by the NOAA/OAR/ESRL PSD, Boulder, Colorado, USA, from their Web site at *http://www.esrl.noaa.gov/psd/*, and ohter information such as earth's bathymetric, topologic and satellite images, was provided by the NASA's Earth Observatory from their web site *http://earthobservatory.nasa.gov/*.

REFERENCES

Cabral, B. and Leedom, L. (1993). Imaging vector fields using line integral convolution. In *Proceedings of the 20th annual conference on Computer graphics and interactive techniques*, pages 263–270. ACM.

Callieri, M., Andrei, R., Di Benedetto, M., Zoppè, M., and Scopigno, R. (2010). Visualization methods for molecular studies on the web platform. In *Proceedings of the 15th International Conference on Web 3D Technology*, pages 117–126. ACM.

Congote, J., Segura, A., Kabongo, L., Moreno, A., Posada, J., and Ruiz, O. (2011). Interactive visualization of volumetric data with webgl in real-time. In *Proceedings of the 16th International Conference on 3D Web Technology*, pages 137–146. ACM.

Forssell, L. and Cohen, S. (1995). Using line integral convolution for flow visualization: Curvilinear grids, variable-speed animation, and unsteady flows. *Visualization and Computer Graphics, IEEE Transactions on*, 1(2):133–141.

Hankin, S., Blower, J., Carval, T., Casey, K., Donlon, C., Lauret, O., Loubrieu, T., Srinivasan, A., Trinanes, J., Godoy, O., et al. (2010). Netcdf-cf-opendap: Standards for ocean data interoperability and object lessons for community data standards processes. In *Oceanobs 2009, Venice Convention Centre, 21-25 septembre 2009, Venise*.

Hlawatsch, M., Sadlo, F., and Weiskopf, D. (2011). Hierarchical line integration. *Visualization and Computer Graphics, IEEE Transactions on*, (99):1–1.

Kenwright, D. and Mallinson, G. (1992). A 3-d streamline tracking algorithm using dual stream functions. In *Proceedings of the 3rd conference on Visualization'92*, pages 62–68. IEEE Computer Society Press.

Klassen, R. and Harrington, S. (1991). Shadowed hedgehogs: A technique for visualizing 2d slices of 3d vector fields. In *Proceedings of the 2nd conference on Visualization'91*, pages 148–153. IEEE Computer Society Press.

Lane, D. (1994). Ufat: a particle tracer for time-dependent flow fields. In *Proceedings of the conference on Visualization'94*, pages 257–264. IEEE Computer Society Press.

Laramee, R., Hauser, H., Doleisch, H., Vrolijk, B., Post, F., and Weiskopf, D. (2004). The state of the art in flow visualization: Dense and texture-based techniques. In *Computer Graphics Forum*, volume 23, pages 203–221. Wiley Online Library.

Liu, Z. and Moorhead, R. (2005). Accelerated unsteady flow line integral convolution. *IEEE Transactions on Visualization and Computer Graphics*, pages 113–125.

Liu, Z. and Moorhead II, R. (2004). Visualizing time-varying three-dimensional flow fields using accelerated uflic. In *The 11th International Symposium on Flow Visualization*, pages 9–12. Citeseer.

McLoughlin, T., Laramee, R., Peikert, R., Post, F., and Chen, M. (2010). Over two decades of integration-based, geometric flow visualization. In *Computer Graphics Forum*, volume 29, pages 1807–1829. Wiley Online Library.

Van Wijk, J. (2002). Image based flow visualization. In *ACM Transactions on Graphics (TOG)*, volume 21, pages 745–754. ACM.

Van Wijk, J. (2003). Image based flow visualization for curved surfaces. In *Proceedings of the 14th IEEE Visualization 2003 (VIS'03)*, page 17. IEEE Computer Society.